Substitution Mechanism of Mn and Fe Ions in $Bi_4Ti_3O_{12}$

Kazuma Nishimura[1], Tsuyoshi Yoshioka[1], and Tomoyuki Yamamoto[1,2]

[1]Faculty of Science and Engineering, Waseda University, Tokyo 169-8555, Japan
[2]Institute of Condensed-Matter Science, Waseda University, Tokyo 169-8555, Japan

Single-phased polycrystalline Mn- and Fe-doped $Bi_4Ti_3O_{12}$ were fabricated using a solid-state reaction technique, doping with various concentrations of Mn and Fe ions. Substitution mechanism of Mn and Fe ions in $Bi_4Ti_3O_{12}$ were investigated with X-ray absorption near-edge structure (XANES) measurements and first-principles calculations. The valence states of the Mn and Fe ions are 4+ and 3+, respectively, inferred from the $L_{2,3}$-edge XANES profiles. From the K-edge XANES analysis, it is determined that Mn and Fe ions are substituted at one of the Ti sites, i.e., Ti(2a) or Ti(4e) sites. Our first-principles total electronic energy calculations suggest that Mn ions are likely to substitute at Ti(2a) sites rather than at Ti(4e) sites, whereas the opposite is true for Fe substitution. Taken together, these results give a clear description of the locations and charge states of the Mn and Fe dopants in $Bi_4Ti_3O_{12}$.

Index Terms— **Bismuth titanate, first-principles calculation, substitution mechanism, X-ray absorption near-edge structure (XANES).**

I. Introduction

BISMUTH titanate ($Bi_4Ti_3O_{12}$) is an attractive lead-free substitute for the materials commonly used in ferroelectric random access memory (FeRAM), and its crystal structure and ferroelectric properties have been extensively studied [1], [2]. Doping techniques can enhance the ferroelectric properties or alter the Curie temperature of $Bi_4Ti_3O_{12}$ FeRAM materials, and results indicate that rare-earth-doped $Bi_4Ti_3O_{12}$ shows significant improvement in ferroelectric properties [3]–[5]. In addition to rare-earth doping, simultaneous doping with 3d transition elements, such as Mn, has also proven effective [6].

Recently, it was reported that Fe-doped $Bi_4Ti_3O_{12}$ exhibits both ferroelectric and ferromagnetic properties, i.e., the multiferroic property, and this property of Fe-doped $Bi_4Ti_3O_{12}$ has been extensively studied [7]. It is essential to know the valence states and the local environment of Mn and Fe ions in $Bi_4Ti_3O_{12}$ in order to understand their influence on the ferroelectric and ferromagnetic properties. However, the local environment of the substitutional Mn and Fe ions has not yet been clearly determined. Techniques, such as the $L_{2,3}$-edge XANES analysis [8]–[11] and the K-edge XANES analysis, along with first-principles calculations, are powerful tools for determining the local environment of 3d transition elements [12], [13]. This combined strategy has been applied to analyze the dopant structure in various types of functional materials, and has successfully determined the local environment for some kinds of dilute dopants [14], [15].

In this paper, we investigate the substitution mechanism of Mn and Fe ions using X-ray absorption near-edge structure (XANES) measurements alongside first-principles calculations. We determined the valence states using the $L_{2,3}$-edge XANES spectra, and the local structure around the Mn and Fe ions by comparing the K-edge XANES spectra with the calculated XANES spectra. Additionally, we computed the total electronic energies of the Mn- and Fe-doped systems to estimate the most energetically favorable sites for substitution.

Manuscript received November 9, 2013; accepted January 6, 2014. Date of current version June 6, 2014. Corresponding author: T. Yamamoto (e-mail: tymmt@waseda.jp).

Color versions of one or more of the figures in this paper are available online at http://ieeexplore.ieee.org.

Digital Object Identifier 10.1109/TMAG.2014.2301447

II. Experimental Procedures

Mn and Fe doped $Bi_4Ti_3O_{12}$ were prepared by the solid state reaction method changing the concentration of Mn and Fe ions, i.e., $x = 0.00, 0.01, 0.03$, and 0.05 in $Bi_4(Ti_{1-x}TM_x)_3O_{12}$ where TM = Mn or Fe. Our raw materials were reagent-grade Bi_2O_3, TiO_2, α-Fe_2O_3, and Mn_2O_3. We mixed these powders in an agate mortar, then calcined them at 1023 K for 5 h in air. These calcined powders were ground and mixed again, and pressed into a cylindrical pellet form (10 mmϕ). We sintered these powder aggregates at 1223 K for 5 h in air. The crystal structures of all samples were verified using the powder X-ray diffraction (XRD) technique with Cu-Kα X-rays.

Mn- and Fe-$L_{2,3}$ XANES spectra were measured at BL-4B in Ultraviolet Synchrotron Orbital Radiation Facility (UVSOR), Okazaki, Japan, using the total electron yield method. This method is effective to measure low-energy XANES spectra, because such low-energy X-rays are absorbed much when the transmission method is used. The X-rays from the storage ring were monochromatized by a varied-line-spacing plane grating (800 lines/mm), and we set the energy resolution of the incident beams ($E/\Delta E$) to 3000 by tuning the slit height at the upper and lower reaches of the grating. Mn- and Fe-K XANES spectra were collected at BL01B1 in SPring-8, Harima, Japan, using a transmission method. The incident beam from the storage ring was monochromatized by a Si(111) double-crystal monochromater. All the XANES measurements were carried out at room temperature.

III. Results and Discussion

The XRD patterns collected from the $Bi_4(Ti_{1-x}Mn_x)_3O_{12}$ and $Bi_4(Ti_{1-x}Fe_x)_3O_{12}$ specimens are shown in Fig. 1(a) and (b), respectively, together with the established XRD pattern of orthorhombic $Bi_4Ti_3O_{12}$ (JCPDS 35-0795). All the diffraction peaks could be indexed as orthorhombic $Bi_4Ti_3O_{12}$, and no extra peaks were found in the collected XRD patterns. The lattice parameters of our samples were calculated using the conventional least-square fitting method to the observed XRD patterns. The lattice parameters and the corresponding volumes of the unit cells are plotted in Fig. 2. These data are also summarized in Table I. All of the lattice constants, a, b, and c, of Mn-doped $Bi_4Ti_3O_{12}$ decreased with increasing Mn concentration, whereas a decreased and b and c

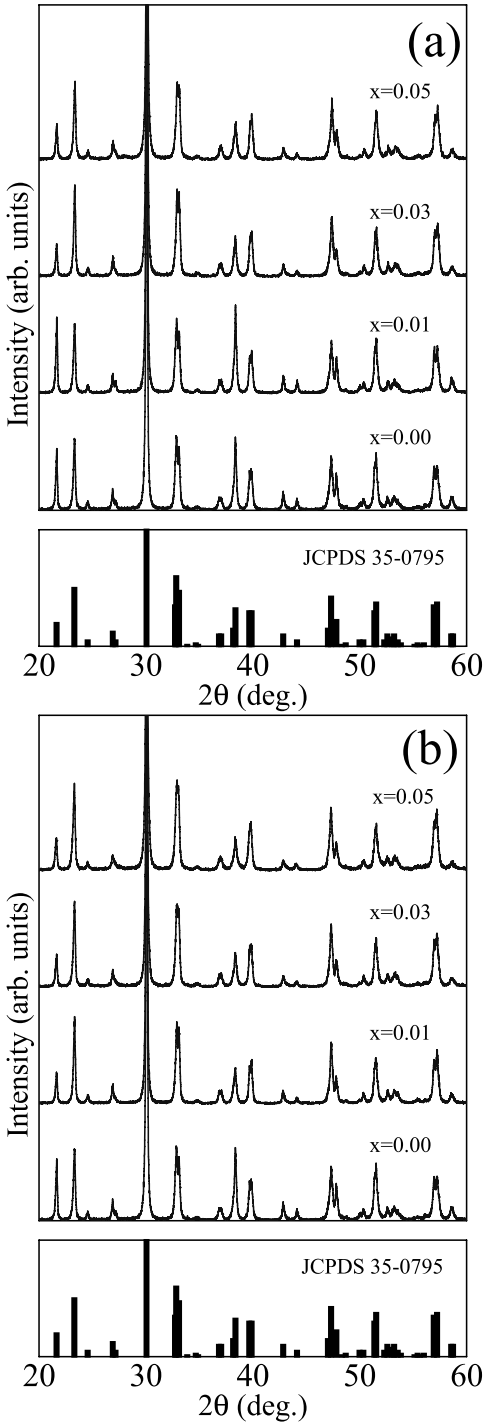

Fig. 1. Observed XRD patterns of (a) $Bi_4(Ti_{1-x}Mn_x)_3O_{12}$ and (b) $Bi_4(Ti_{1-x}Fe_x)_3O_{12}$. Calculated XRD pattern of $Bi_4Ti_3O_{12}$ (JCPDS 35-0795) is included at the bottom of each pattern group.

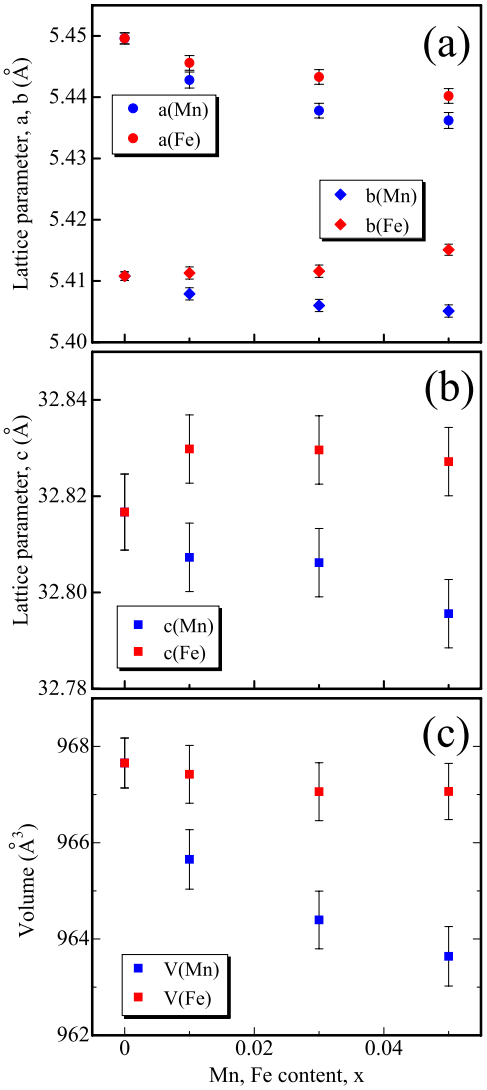

Fig. 2. Lattice constants (a) a and b, (b) c, and (c) volume V of $Bi_4(Ti_{1-x}Mn_x)_3O_{12}$ and $Bi_4(Ti_{1-x}Fe_x)_3O_{12}$ obtained from the XRD patterns as a function of dopant content.

TABLE I
LATTICE PARAMETERS AND VOLUMES OF $Bi_4(Ti_{1-x}M_x)_3O_{12}$ (M = Mn, Fe)

	x	a (Å)	b (Å)	c (Å)	V (Å^3)
pure	0	5.4496	5.4108	32.8167	967.66
Mn-doped	0.01	5.4428	5.4079	32.8073	965.65
	0.03	5.4378	5.4060	32.8062	964.40
	0.05	5.4362	5.4051	32.7956	963.64
Fe-doped	0.01	5.4456	5.4113	32.8298	967.42
	0.03	5.4433	5.4116	32.8296	967.06
	0.05	5.4402	5.4151	32.8272	967.06

increased as the Fe concentration increased. The volumes of both Mn- and Fe-doped $Bi_4Ti_3O_{12}$ unit cells decreased as the concentration of the dopant increased, though this volume reduction is much smaller in the Fe-doped ones. These results indicate that both Mn and Fe ions appear to be substituted at one of the cation sites, i.e., Bi or Ti sites.

Ionic radii for various ions in this system [16] are listed in Table II. If Mn and Fe ions substitute at Bi sites, unit cell volume should decrease much since all the ionic radii with different valences are much smaller than that of Bi^{3+}. In the case of the substitution at Ti sites, only Fe^{4+} and Mn^{4+} can produce the experimentally observed reduction of volumes. However, the formation of an oxygen vacancy may appear for charge compensation in the crystal when trivalent Mn and Fe ions substitute at Ti^{4+} site, which may also lead to the reduction of the volume. Thus, an analysis of the doped crystal structure based on ionic substitutions alone cannot determine the substitution sites for Mn and Fe ions in $Bi_4Ti_3O_{12}$.

TABLE II
IONIC RADII OF CATIONS WITH SIX-COORDINATION [16]

ion	ionic radius $\AA$
Bi^{3+}	1.030
Mn^{2+}	0.830
Fe^{2+}	0.780
Mn^{3+}	0.645
Fe^{3+}	0.645
Ti^{4+}	0.605
Fe^{4+}	0.585
Mn^{4+}	0.530

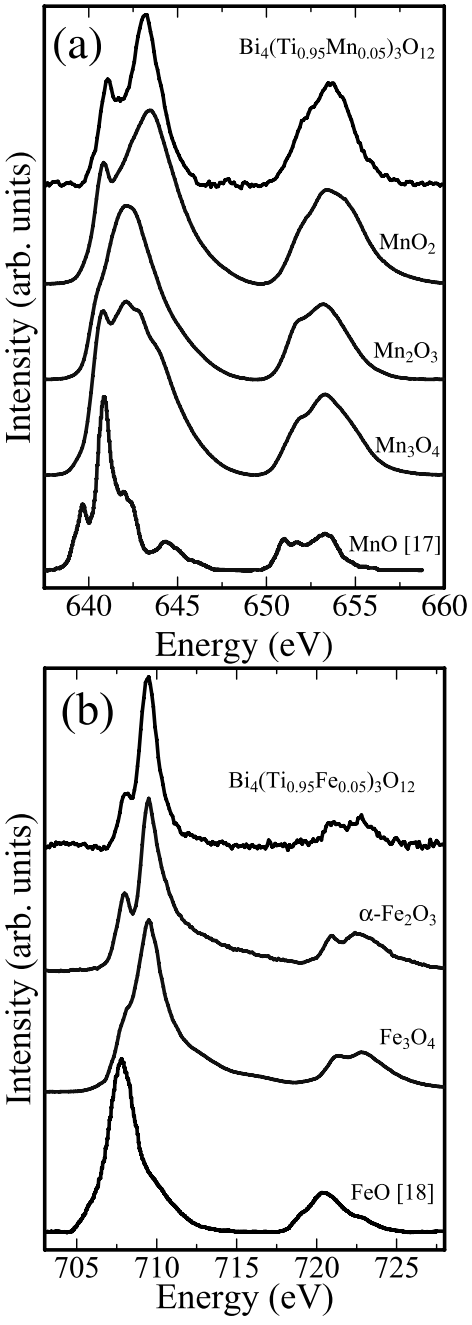

Fig. 3. Observed $L_{2,3}$-edge XANES spectra for (a) Mn-doped and (b) Fe-doped $Bi_4Ti_3O_{12}$. The corresponding spectra of Mn and Fe oxides are also plotted for comparison.

We employed the Mn- and Fe-$L_{2,3}$ XANES spectra to determine the valence state of doped Mn and Fe ions; these are in Fig. 3, shown alongside the spectra of Mn and Fe oxides.

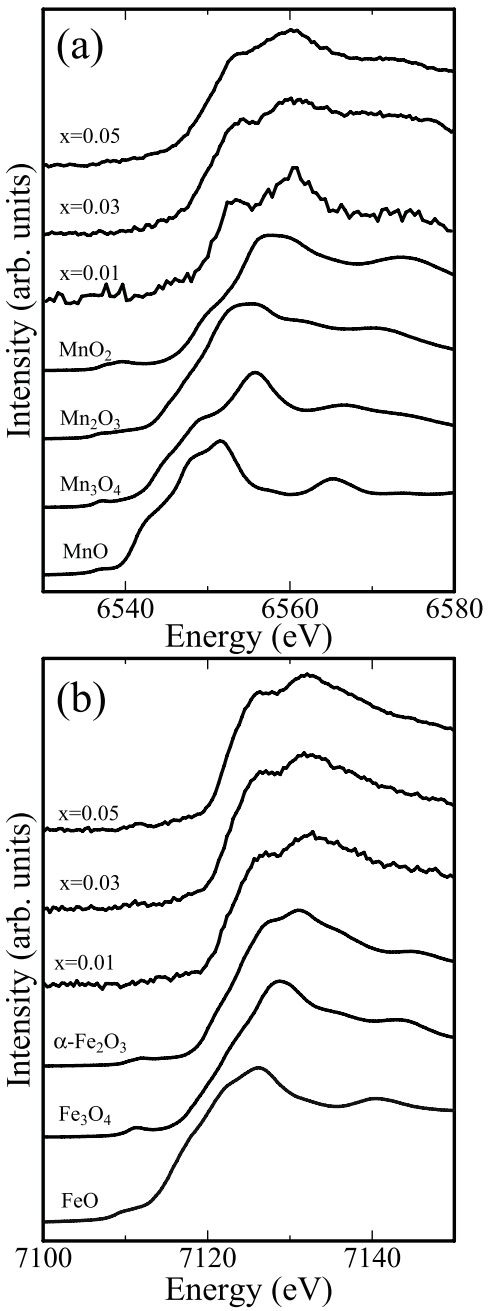

Fig. 4. Observed K-edge XANES spectra for (a) Mn-doped and (b) Fe-doped $Bi_4Ti_3O_{12}$. The corresponding spectra of Mn and Fe oxides are also plotted for comparison.

In general, $L_{2,3}$-edge XANES spectra of 3d transition metal is quite sensitive to change in valence state, since they can be obtained from the electric dipole transition from 2p to 3d states. In addition, profiles of $L_{2,3}$ XANES spectra can strongly reflect only nearest neighboring coordinations, since 3d orbital is a localized orbital. Then, we are able to use the fingerprint type analysis by comparing the spectrum of interest with standard oxides to determine the valence state of 3d transition elements. From the comparison of our observed Mn-$L_{2,3}$ spectra with those of the reference Mn oxides, we observe that the spectral fine structures of Mn ions in $Bi_4Ti_3O_{12}$ [Fig. 3(a)] show a similar profile to those of MnO_2, which indicates to us that the majority of Mn ions in $Bi_4Ti_3O_{12}$ exist as Mn^{4+}. On the other hand, the Fe-$L_{2,3}$ XANES profile of Fe ions in $Bi_4Ti_3O_{12}$ [Fig. 3(b)] is

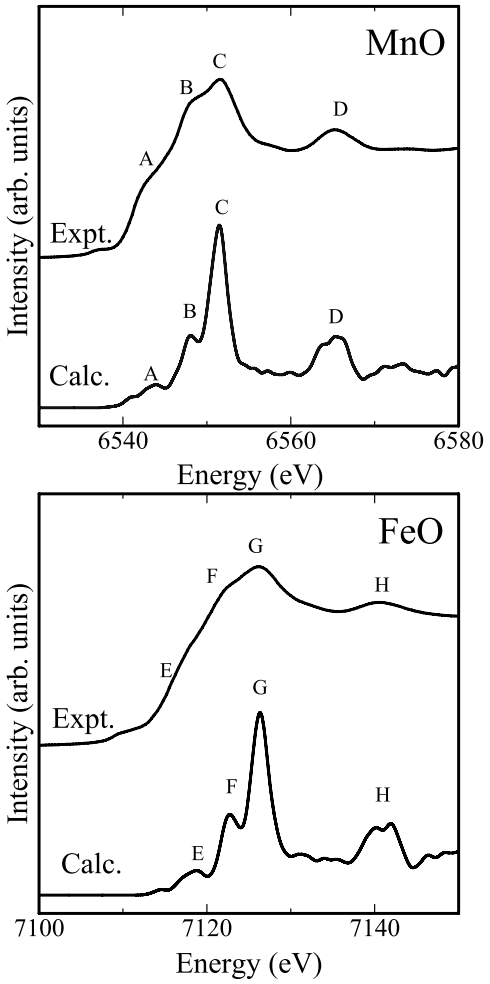

Fig. 5. Comparison of K-edge XANES spectra between experiments and calculations of (a) MnO and (b) FeO.

similar to that of α-Fe_2O_3, which suggests that most Fe ions in $Bi_4Ti_3O_{12}$ are in the 3+ state.

Our observed Mn and Fe K-edge XANES spectra of Mn- and Fe-doped $Bi_4Ti_3O_{12}$ are in Fig. 4, alongside those of standard Mn and Fe oxides. The spectral fine structures of Mn and Fe in $Bi_4Ti_3O_{12}$ are different from any of the spectra of standard Mn and Fe oxides, which indicates Mn and Fe ions do not exist as simple oxides and the local environments of Mn and Fe ions are different from those in Mn and Fe oxides. This type of experimental comparison alone cannot determine the local environment of the doped ions in the case of K-edge XANES analysis, because K-edge XANES profile is a reflection of unoccupied p-states, which is rather delocalized than d-states. Then, no standard spectra are available to be compared with the experimental spectrum of interest. Therefore, the additional information provided by theoretical calculations is required to resolve the final doped structure. These theoretical fingerprints can be compared with the observed XANES spectrum of interest to help identify the local environment of doped ions.

We performed these first-principles calculations to construct theoretical Mn-K and Fe-K XANES spectra of Mn- and Fe-doped $Bi_4Ti_3O_{12}$, respectively. All the calculations were carried out using the augmented plane wave plus local orbital (APW+lo) solution of the Kohn–Sham equations, as implemented in the WIEN2k package [19]. The core-hole effect was directly introduced to fix the final state of the X-ray absorption

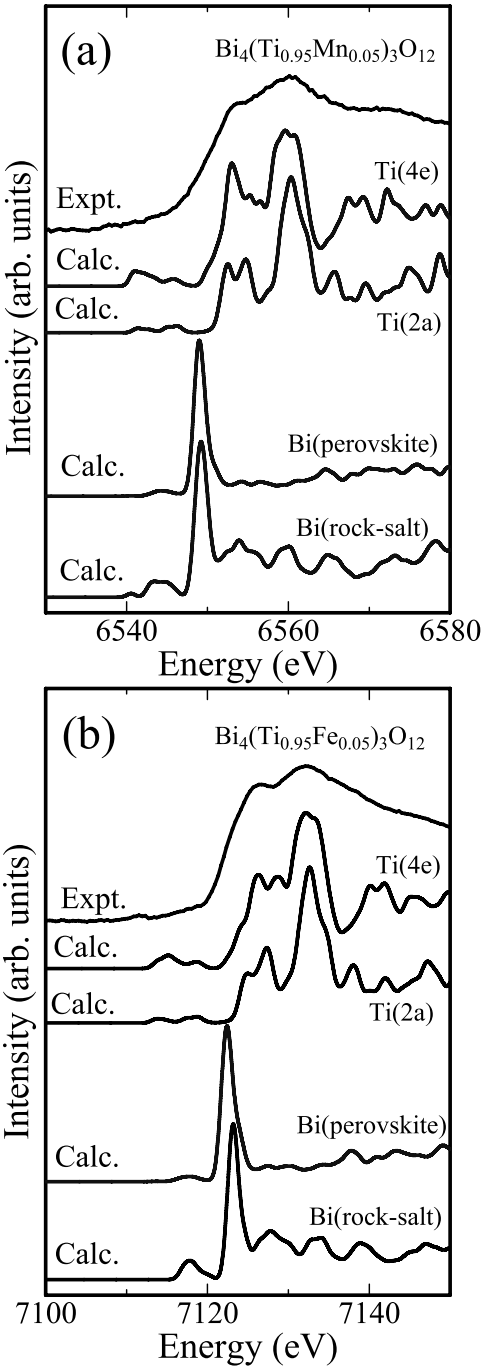

Fig. 6. Comparisons of K-edge XANES spectra between experiments and calculations of (a) Mn-doped and (b) Fe-doped $Bi_4Ti_3O_{12}$.

process by removing one electron from the K-shell of Mn or Fe and placing an additional electron at the bottom of the unoccupied band, which is approximately correspond to the final states of Mn and Fe K-edge X-ray absorption process. We determined the energies associated with the calculated XANES spectra by taking the difference in total electronic energy of the initial (ground) and final (core-hole) states of the Mn and Fe K-edge X-ray absorption process.

Prior to the calculation of the Mn- and Fe-doped $Bi_4Ti_3O_{12}$, theoretical XANES spectra of MnO and FeO with a rock-salt structure were calculated using the $2 \times 2 \times 2$ supercell (64 atoms) of conventional unit-cell. The muffin-tin radii, R_{MT}s, of Mn, Fe, and O were set to 1.98, 1.98, and 1.30 a.u.,

respectively, and the plane wave cutoff K_{max} was 3 $Ry^{1/2}$. A $3 \times 3 \times 3$ k-point mesh based on the Monkhorst–Pack scheme [20] was sampled in reciprocal space. The calculated spectra were broadened using a Gaussian function with width 1.16 and 1.25 eV for Mn and Fe K-edges, respectively. These peak broadenings correspond to the lifetime of a K core-hole [21]. We employed a generalized gradient approximation [22] for the exchange-correlation functional.

The calculated XANES spectra of MnO and FeO are compared to the experiments in Fig. 5(a) and (b), respectively. Characteristic features of XANES spectra of MnO and FeO were well reproduced by our calculations when the energy was corrected by 21.5 eV ($\Delta E/E = 0.3\%$) for MnO and 21.6 eV ($\Delta E/E = 0.3\%$) for FeO. It is noted here that the calculated spectra are sharper than the experimental ones. This is because the calculated spectra were broadened by taking only lifetime broadening effect but not taking the spectrometer broadening into considerations. We built super-cells for Mn- and Fe-doped $Bi_4Ti_3O_{12}$ by expanding the unit-cell of $Bi_4Ti_3O_{12}$ with a space group of I4/mmm along the *b*-axis twice, i.e., a $1 \times 2 \times 1$ super-cell (76 atoms). From the results of Mn- and Fe-$L_{2,3}$ XANES analysis, valence states of Mn and Fe ions in $Bi_4Ti_3O_{12}$ have been determined to be 4+ and 3+, respectively. Then, we constructed the models in which the Mn^{4+} and Fe^{3+} ions were substituted at Bi or Ti sites.

There are two crystallographically independent sites for Bi (i.e., in a perovskite-type layer or a rock-salt-type layer) and two independent sites for Ti [i.e., Ti(2a) and Ti(4e)]. We constructed eight types of models by replacing one of the Bi or Ti ions in one of these configurations by a Mn^{4+} or Fe^{3+} ion and by controlling the total number of electrons in the cell. When a Bi^{3+} ion was replaced by Mn^{4+} ion, for instance, one electron was removed from the cell at initial condition. Spectral energies were shifted by the same amounts as for the case of MnO and FeO, i.e., 21.5 and 21.6 eV, respectively.

Calculated XANES profiles of Mn- and Fe-doped $Bi_4Ti_3O_{12}$ are compared with our experimental profiles in Fig. 6(a) and (b), respectively. In both figures, the calculated XANES spectra of Bi site models show significant differences compared with the observed profiles. On the other hand, both of the calculated spectra of the two types of the Ti site substitution models reproduce the experimental data well. It should be noted here that the spectral signatures of the Ti(4e) and Ti(2a) models are quite similar, which suggests the local environments of Mn ions are quite similar when they are substituted at Ti(2a) and Ti(4e) sites.

Unfortunately, the theoretical XANES fingerprints cannot determine which Ti site is preferable for the substitution of Mn and Fe ions in $Bi_4Ti_3O_{12}$. To determine the specific sites for substitution, we compared the total electronic energies calculated above for the calculations of spectral energies. In the case of Mn substitution, the total electronic energy is lower by 0.16 eV/cell when Mn is substituted at Ti(2a) site than at Ti(4e), whereas that is lower by 0.30 eV/cell when Fe ion is at Ti(4e) site than at Ti(2a). This is an indication that Mn and Fe ions substitute at Ti(2a) and Ti(4e) sites, respectively.

IV. Conclusion

We synthesized polycrystalline Mn- and Fe-doped $Bi_4Ti_3O_{12}$ specimens using a solid-state reaction method with different concentrations of Mn and Fe ions: $x = 0.00, 0.01, 0.03$, and 0.05 in $Bi_4(Ti_{1-x}Mn_x)_3O_{12}$ and $Bi_4(Ti_{1-x}Fe_x)_3O_{12}$, respectively. The crystal structures of all samples were verified by powder XRD technique, which show all the samples possessed a single-phase orthorhombic structure equivalent to $Bi_4Ti_3O_{12}$. Substitution mechanism of Mn and Fe ions in $Bi_4Ti_3O_{12}$ was investigated by XANES analysis with the aid of the first-principles calculations. Mn- and Fe-$L_{2,3}$ XANES measurements determined the valence states of the Mn and Fe ions as 4+ and 3+, respectively. K-edge XANES analysis with the aid of the first-principles calculations revealed that Mn and Fe ions should substitute at Ti site. Finally, the first-principles total electronic energy calculations suggest that Mn and Fe ions should substitute at Ti(2a) and Ti(4e) sites, respectively.

Acknowledgment

The authors would like to thank E. Shigemasa, H. Iwayama, E. Nakamura, and N. Kondo of UVSOR for their assistance with the Mn- and Fe-$L_{2,3}$ XANES measurements. The Mn- and Fe-$L_{2,3}$ XANES measurements was supported by BL-4B in UVSOR through the Institute of Molecular Science under Proposal 24-517, 25-519. The Mn-K and Fe-K XANES measurements was supported by BL01B1 in SPring- 8 through the Japan Radiation Research Institute under Proposal 2013A1034.

References

[1] S. E. Cummins and L. E. Cross, "Electrical and optical properties of ferroelectric $Bi_4Ti_3O_{12}$ single crystals," *J. App. Phys.*, vol. 39, no. 5, pp. 2268–2274, 1968.

[2] J. F. Dorrian, R. E. Newnham, and D. K. Smith, "Crystal structure of $Bi_4Ti_3O_{12}$," *Ferroelectr.*, vol. 3, no. 1, pp. 17–27, 1971.

[3] B. H. Park, B. S. Kang, S. D. Bu, T. W. Noh, J. Lee, and W. Jo, "Lanthanum-substituted bismuth titanate for use in non-volatile memories," *Nature*, vol. 401, pp. 682–684, Oct. 1999.

[4] Y. Noguchi, I. Miwa, Y. Goshima, and M. Miyayama, "Defect control for large remanent polarization in bismuth titanate ferroelectrics doping effect of higher-valent cations," *Jpn. J. Appl. Phys.*, vol. 39, pp. L1261–L1262, Nov. 2000.

[5] T. Kojima, T. Watanabe, H. Funakubo, K. Saito, M. Osada, and M. Kakihara, "Ferroelectric properties of lanthanide-substituted $Bi_4Ti_3O_{12}$ epitaxial thin films grown by metalorganic chemical vapor deposition," *J. App. Phys.*, vol. 93, no. 3, pp. 1707–1712, 2003.

[6] J. P. Kim, J. Y. Hwang, C. R. Cho, M. K. Ryu, M. S. Jang, and S. Y. Jeong, "Ferroelectric properties of Mn-doped $Bi_{3.6}La_{0.4}Ti_3O_{12}$ thin films prepared under different annealing conditions," *Jpn. J. Appl. Phys.*, vol. 43, no. 9B, pp. 6590–6593, 2004.

[7] X. Q. Chen, F. J. Yang, W. Q. Cao, H. Wang, C. P. Yang, D. Y. Wang, *et al.*, "Enhanced multiferroic characteristics in Fe-doped $Bi_4Ti_3O_{12}$ ceramics," *Solid State Commun.*, vol. 150, no. 27, pp. 1221–1224, 2010.

[8] H. Ikeno, F. M. F. de Groot, E. Stavitski, and I. Tanaka, "Multiplet calculations of $L_{2,3}$ x-ray absorption near-edge structures for 3D transition-metal compounds," *J.Phys., Condensed Matter*, vol. 21, no. 10, pp. 104208-1–104208-17, 2009.

[9] Y. Kumagai, H. Ikeno, F. Oba, K. Matsunaga, and I. Tanaka, "Effects of crystal structure on Co-$L_{2,3}$ x-ray absorption near-edge structure and electron-energy-loss near-edge structure of trivalent cobalt oxides," *Phys. Rev.*, vol. 77, no. 15, pp. 155124-1–155124-9, 2008.

[10] H. Ikeno, T. Mizoguchi, and I. Tanaka, "Ab initio charge transfer multiplet calculations on the $L_{2,3}$ XANES and ELNES of 3D transition metal oxides," *Phys. Rev.*, vol. 83, pp. 155107-1–155107-13, 2011.

[11] T. Yoshioka, T. Yamamoto, and A. Kitada, "Co-L_3 X-ray absorption near-edge structure analysis of $Pr_{1-x}Ca_xCoO_{3-\delta}$ and $Pr_{1-x}Sr_xCoO_{3-\delta}$," *Physica*, vol. 407, no. 21, pp. 4114–4116, 2012.

[12] T. Yamamoto, Y. Kawashima, Y. Kusakabe, S. Matsuda, Y. Mizuoka, Y. Nakade, *et al.*, "Local environment analysis of dopants in ceramics by x-ray absorption near-edge structure with the aid of first-principles calculations," *J. Phys., Condensed Matter*, vol. 21, no. 10, pp. 104211-1–104211-8, 2009.

[13] T. Yoshioka, T. Yamamoto, and A. Kitada, "Analysis of charge compensation mechanisms in $Pr_{1-x}A_xCoO_{3-\delta}$ (A = Ca, Sr) by X-ray absorption near-edge structure," *Jpn. J. App. Phys.*, vol. 51, no. 7R, pp. 073201-1–073201-4, 2012.

[14] I. Tanaka, T. Mizoguchi, M. Matsui, S. Yoshioka, H. Adachi, T. Yamamoto, *et al.*, "Identification of ultradilute dopants in ceramics," *Nature Mater.*, vol. A107, no. 8, pp. 541–545, 2003.

[15] I. Tanaka, T. Mizoguchi, and T. Yamamoto, "XANES and ELNES in ceramic science," *J. Amer. Ceram. Soc.*, vol. 88, no. 8, pp. 2013–2029, 2005.

[16] R. D. Shannon, "Revised effective ionic radii and systematic studies of interatomic distances in halides and chalcogenides," *Acta Cryst.*, vol. A32, pp. 751–767, Sep. 1976.

[17] B. Gilbert, B. H. Frazer, A. Belz, P. G. Conrad, K. H. Nealson, D. Haskel, *et al.*, "Multiple scattering calculations of bonding and X-ray absorption spectroscopy of manganese oxides," *J. Phys. Chem.*, vol. 107, no. 16, pp. 2839–2847, 2003.

[18] T. J. Regan, H. Ohldag, C. Stamm, F. Nolting, J. Luning, J. Stohr, *et al.*, "Chemical effects at metal/oxide interfaces studied by x-ray-absorption spectroscopy," *Phys. Rev.*, vol. B64, pp. 214422-1–214422-11, Nov. 2001.

[19] P. Blaha, K. Schwarz, G. K. H. Madsen, D. Kvasnicka, and J. Luitz, *WIEN2k, An Augmented Plane Wave + Local Orbitals Program for Calculating Crystal Properties*. Wien, Austria: Univ. Vienna, 2001.

[20] H. J. Monkhorst and J. D. Pack, "Special points for Brillonin-zone integrations," *Phys. Rev.*, vol. B13, no. 12, pp. 5188–5192, 1976.

[21] M. O. Krause and J. H. Oliver, "Natural widths of atomic K and L levels, Kα X-ray lines and several KLL Auger lines," *J. Phys. Chem. Ref. Data*, vol. 8, no. 2, pp. 329–338, 1979.

[22] J. P. Perdew, K. Burke, and M. Ernzerhof, "Generalized gradient approximation made simple," *Phys. Rev. Lett.*, vol. 77, no. 18, pp. 3865–3868, 1996.